

Edge effect compensation for citrus canker lesion detection due to light source variation – a hyperspectral imaging application

Nikhil P. Niphadkar^{1*}, Thomas F. Burks², Jianwei Qin³, Mark Ritenour⁴

(1. ATW Automation Inc., 526 Wiltshire Blvd. Apt. - A, Dayton, OH 45419;

2. Department of Agricultural & Biological Engineering, University of Florida, P.O. Box 110570, Gainesville, FL 32611-0570;

3. United States Department of Agriculture, 10300 Baltimore Avenue Building 303 BARC-East, Room 0151 Beltsville, MD 20705-2350;

4. Department of Horticultural Sciences, University of Florida, 2199 South Rock Road Fort Pierce, FL 34945-3138)

Abstract: The spread of citrus canker has become one of the most important challenges faced by Florida Fresh Market citrus is affecting the export of citrus fruits to several international markets including European countries. Previous studies have shown that automated detection systems can help detect citrus canker infected fruit and could assist in eliminating the detected fruit from shipment to closed markets. Most automated detection systems use some form of machine vision with artificial light sources. However, when capturing images of spherical objects, non-uniform illumination results in an edge blackening effect resulting in higher misclassification rate. The basic objective of this research was to implement a compensation algorithm to eliminate the edge effect when capturing hyperspectral image of citrus fruits. The algorithm originally developed by Gomez et al. 2007, was adapted for the purpose of canker detection. The image was corrected for spatial variations (flat field correction) caused by intensity of light source as well as geometrical variation caused by the spherical geometry of the citrus fruit. In this study, the geometric correction was accomplished by constructing a 3-D digital elevation model (DEM) of the fruit from its 2-D image. This DEM provided the geometric properties of the fruit X, Y, and Z coordinates which were exploited in the course of estimating the geometric correction factor for each pixel. The corrected image portrayed a more uniform brightness of the citrus fruit surface throughout. Tests were conducted on 10 orange samples (five marketable and five cankerous) to validate the results of the algorithm which demonstrated that the geometric correction resulted in uniform intensity of radiation throughout the fruit surface thus reducing the within class variation.

Keywords: edge effect compensation, hyperspectral imaging, canker, spatial correction, geometric correction

Citation: Niphadkar, N., T. Burks, J. Qin, and M. Ritenour. 2013. Edge effect compensation for citrus canker lesion detection due to light source variation - A hyperspectral imaging application. *Agric Eng Int: CIGR Journal*, 15(4): 314–327.

1 Introduction

The citrus industry is a vital part of the State of Florida's economy producing approximately 70% of the overall citrus supply for the United States. Among others, citrus canker is one of the biggest problems facing the fresh market in citrus industry in Florida. Canker can spread rapidly under certain conditions and can affect the export of citrus to canker free areas. In the fall of

2009, joint efforts of United States Department of Agriculture (USDA) and Animal and Plant Health Inspection Service (APHIS) concluded that canker couldn't be transmitted by infected fruit when treated with proper disinfectants. This resulted in an opening of trade of canker infected fruits within the United States, relieving the pressure off the Florida citrus grower to some extent. However there remained a few European markets which still didn't accept canker infected shipments. A solution to this problem could be detecting canker in the packaging house and eliminating infected fruit from the pack out. In recent years, machine vision based approaches have proven successful

Received date: 2012-09-28 Accepted date: 2013-10-20

*Corresponding author: Nikhil P. Niphadkar, ATW Automation Inc., 526 Wiltshire Blvd. Apt. - A, Dayton, OH45419. Email: nniphadkar@atwautomation.com, Tel: (937) 516-5140.

in on-line grading of fruit and vegetable blemishes and defects. In addition, hyperspectral and multispectral techniques have proven effective for detecting blemishes, defects and even fecal matter on fruits and vegetables.

Essentially all computer vision applications include some type of camera to capture images of the objects which are later processed further for defective detection. The distribution of light reflected by the objects and captured by the system camera greatly depends on the position of the light source as well as the geometry of the object. The images captured typically undergo calibration to rectify spectral as well as spatial inhomogeneities caused by the lighting system. This calibration is usually based on a plane model correction utilizing a calibrating material with known reflectance. When the object being captured is flat by geometry, the above method works perfectly fine. In case of spherical objects, the reflection of light causes the edges of the object to appear darker while the central area appears brighter (Gomez et al., 2007; Unay and Gosselin, 2007; Aleixos et al., 2002). This edge effect is always experienced during the inspection of citrus fruits, apples, tomatoes, peaches, etc., which are more or less spherical in shape. If the illumination system is improperly implemented it may also cause the edge effect. In many cases this edge effect leads the classification algorithm to draw wrong conclusions by identifying this darkened peel at the edge of the fruit as diseased or defective. There is also a possibility that the edge pixels may contain useful information which could be lost if a masking operation was employed. It has been suggested that adding additional light sources on the sides of the fruit along with the one on top may remove the edge effect. However, these additional light sources may generate shadows on the fruit resulting in non-uniform brightness over the fruit surface. If the illumination system is not efficient enough, it may generate glare or shadows at particular locations of the object being photographed. It should however be noted that it is not always possible to alter the illumination system because of cost or other constraints. In those situations, it becomes necessary to preprocess the images and make them suitable for further analysis by correcting the images for uniform reflectance.

Edge effect may be experienced by visible spectrum computer vision system as well as the hyperspectral imaging system. In hyperspectral imaging, the system will capture numerous images of the same field of view at different wavelengths using a very narrow bandwidth (approximately 10 nm). Hyperspectral imaging systems are very sensitive to the illumination. Hence it becomes necessary to eliminate illumination edge effect, shadows or saturated regions in order to properly investigate disease defects on the surface of a fruit.

Gomez et al. (2007) introduced a technique which considered the geometry of the object and corrected the edge effect. They assumed the spherical object to be a Lambertian surface and produced its digital elevation model (DEM) by predicting the height of each pixel in the 2-D image. Uniform reflection of the light in all directions irrespective of the direction from which it was being observed, was the inherent characteristic of the Lambertian surface. Then they computed a correction factor for each pixel by using the three coordinates (X, Y and height) of each pixel from the digital elevation model. When this correction factor was applied to the original image, the darkening of the edges of the spherical objects vanished, thereby equalizing the grey level of the object surface throughout.

The overall objective of this research was to implement the technique invented by Gomez et al. for edge effect compensation and apply it to citrus fruits to improve the classification rate of citrus canker by avoiding the false positive errors due to edge blackening. Hence the specific objectives were,

- To implement the edge effect compensation algorithm
- To test the effectiveness of the algorithm by conducting extensive experiments by applying it to the citrus fruits
- To evaluate its effectiveness in correcting the edge for canker lesion detection

2 Materials and methods

2.1 Hyperspectral imaging system

A hyperspectral imaging system was used to acquire reflectance images from citrus samples. Schematic

diagram of the system is illustrated in Figure 1. It was a push broom, line-scan based imaging system that utilized an electron multiplying charge-coupled-device (EMCCD) camera (iXon, Andor Technology Inc., South Windsor, CT, USA). The EMCCD had 1004×1002 pixels and was thermoelectrically cooled to -80°C through a double-stage Peltier device. An imaging spectrograph (ImSpector V10E, Spectral Imaging Ltd., Oulu, Finland) and a C-mount zoom lens (Rainbow CCTV H6X8, International Space Optics, S.A., Irvine, CA, USA) were mounted to the camera. The instantaneous field of view (IFOV) was limited to a thin line by the spectrograph aperture slit (30 μm), and the spectral resolution of the imaging spectrograph was 2.8 nm. Through the slit, light from the scanned IFOV line was dispersed by a prism-grating-prism device and projected onto the EMCCD. Therefore, for each line-scan, a two-dimensional (spatial and spectral) image was created with the spatial dimension along the horizontal axis and the spectral dimension along the vertical axis of the EMCCD. The lighting unit consisted of two 21 V, 150 W halogen lamps powered with a DC voltage regulated power supply (TechniQuip, Danville, CA, USA). The light was transmitted through optical fiber bundles toward line light distributors. Two line lights were (BiSlide-MN10, Velmex Inc., Bloomfield, NY, USA) move arranged to illuminate the IFOV. A programmable, motorized positioning table d citrus samples (five for each run) transversely through the line of the IFOV. Twenty two hundred line scans were required for five fruit samples with 460 pixels per scan covering the fruit at each, thus generating a 3-D hyperspectral image cube with the spatial dimension of 2200×460 for each band. In order to validate performance of the algorithm, ten citrus fruit (oranges) samples, five marketable and five cankerous were used for the analysis. When estimating the geometric correction factor, single fruit was separated using ENVI software. Spectral calibration of the system was performed using an Hg-Ne spectral calibration lamp (Oriol Instruments, Stratford, CT, USA). Because of inefficiencies of the system at certain wavelength regions (e.g., low light output in the visible region less than

450 nm, and low quantum efficiency of the EMCCD in the NIR region beyond 930 nm), only the wavelength range between 450 and 930 nm (totaling 92 bands with a spectral resolution of 5.2 nm) was used in this investigation. The parameterization and data-transfer interface software for the hyperspectral imaging system were developed using a SDK (Software Development Kit) provided by the camera manufacturer for Microsoft Visual Basic (Version 6.0) platform in the Windows operating system.

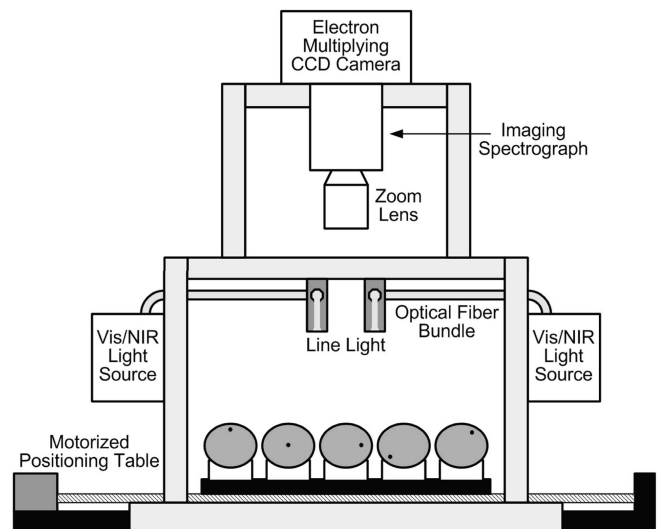


Figure 1 Hyperspectral imaging system for acquisition of reflectance images of grapefruits

2.2 Flat field correction

As mentioned in the earlier paragraph, halogen lamps (21 V, 150 W) were used for the illumination in the hyperspectral imaging system. The problem associated with a halogen lamp was that it suffered with high order of directionality. This resulted in varied intensity of the light source in the plane of the scene which was termed the spatial variation of light source. In order to take care of this issue, the flat field correction was carried out. During flat field correction, the image was pre-processed using a flat white panel of known reflectance. This white panel was usually called a white reference. In this study, a white Spectralon panel was used as a reference. The first step was to perform the correction of the hyperspectral image based on the ratio of reflectance of the fruit ($\rho(\lambda)$) and the radiance of the light source ($I(\lambda)$) as denoted by Equation (1).

$$R\lambda = \rho(\lambda)I(\lambda) \quad (1)$$

where, $R(\lambda)$ is the spatially corrected reflectance image of the fruit. However the reflectance of the fruit ($\rho(\lambda)$) and the radiance of the light source ($I(\lambda)$) cannot be measured as absolute values using the hyperspectral imaging system. Hence in order to achieve this correction the white and dark references were used. Therefore the spatial variation of the light source was rectified using Equation (2):

$$R\lambda = R_s\lambda - R_d(\lambda)R_w\lambda - R_d(\lambda) * \Psi_{Ref} \quad (2)$$

where, λ = Wavelengths; $R_s(\lambda)$ = Original (uncorrected) reflectance image of the fruit; $R_d(\lambda)$ = Reflectance image of dark current; $R_w(\lambda)$ = Reflectance image of white reference; Ψ_{Ref} = Reflectance factor of the white reference panel.

The dark current image $R_d(\lambda)$ was acquired with the light source off and the camera lens covered with the cap and the white reference image $R_w(\lambda)$ was acquired using the white spectralon panel. The actual reflectance factor (Ψ_{Ref}) of the white panel was around 98.5% in the wavelength range covered for the study (450 – 930 nm) however in this exploration for simplicity it was assumed to be 100%. The correction mentioned in the Equation (2) was applied to all the monochrome images in the wavelength range mentioned above. The relative reflectance images, processed using above mentioned procedure, were then multiplied by a factor of 10,000 so as to achieve the pixel values for resultant images in the range 0 to 10,000. This multiplication factor was applied in order to attain the pixel value range comparable to that of the original data from the hyperspectral imaging camera and also to reduce the round off errors for further data analysis. Further details about the flat field correction can be found in Qin et al (2008).

2.3 Image masking

After correcting the images for spatial variation a mask of the fruit image was created for removing the noisy background. The mask template was formed by determining the threshold value by visual inspection of one of the monochrome images (765 nm) that had good contrast between fruit surface and the background. The mask was then applied to extract the fruit pixels and remove the background from all the monochrome images in the hyperspectral image cube. The subsequent

analysis used these masked images for further processing. The algorithms for flat field correction as well as image masking were developed during previous explorations (Qin et al. 2008).

2.4 Derivation of geometric correction factor

In order to remove the blackened edges of the image of citrus fruit due to the edge effect and to make the intensity of the fruit surface uniform throughout, a geometric correction was applied to the image. The expression for the geometric correction factor (ε_g) was derived from the illumination model. The illumination provided to the spherical object by the light source ($I_T(\lambda)$) was modeled as a function of two illumination components, the direct component ($I_D(\lambda)$) and the fuzzy component ($I_F(\lambda)$). As the name suggested the direct component directly came from the light source. The illumination provided by the direct component depended on the angle of incidence (Φ) which was the angle between the beam of direct light and the direction normal to the surface at the point of incidence. On the other hand, fuzzy light was the indirect illumination provided by numerous reflections of the light from the surrounding (i.e., from the walls of the illumination chamber). The model described above can be represented in the mathematical form in the following way (Equation (3)):

$$I_T\lambda = I_D\lambda * \cos\Phi + I_F\lambda \quad (3)$$

It should be noted that the model mentioned in Equation (3) takes into account the geometry of the object. As mentioned earlier we had assumed the surface of the citrus fruit to be a Lambertian surface. This type of surface was recognized by the fact that irrespective of the direction of observation, it reflected the light falling on it in exactly the same way in all the directions and this reflected light obeyed the cosine law by distributing reflected energy in proportion to the cosine of the incidence angle (Φ) (Green and MacDonald 2002). According to Foley et al. (1996) and Gomez et al. (2007), in case of the Lambertian surface, the light received by the viewer depended on the angle of incidence (Φ) (same as what we used in the direct component of the illumination) So it can be concluded that the illumination model described in Equation (3) exactly suits the needs.

If we were to capture the images of the flat surface, with light source located right above the surface, the illumination model mentioned in Equation (3) can be expressed as Equation (4),

$$I\lambda = ID\lambda + IF\lambda \quad (4)$$

where, $I(\lambda)$ is the total average lights which is nothing but radiance of the light source mentioned in Equation (1). In the present study the light source is located right above the object being captured. Hence it should be noted that if the light source was located right above the object, the illumination model no longer depended on the angle of incidence (Φ). When it came to a flat surface, the angle Φ was equal to zero for every point on the surface, making the “ $\cos(\Phi)$ ” term in Equation (3) equal to one every time. So one should keep in mind that Equation (3) and Equation (4) represented the same model while capturing the images of a flat object. However they were potentially different models when it came to capturing a spherical object (provided that the light source was located right above the object being captured).

In order to derive the expression for the geometric correction factor (ε_g), two parameters, α_D and α_F were defined (Equation (5) and Equation (6)). The parameter α_D was the ratio of the direct light ($I_D(\lambda)$) and the total average lights ($I(\lambda)$), while the parameter α_F was the ratio between the fuzzy light ($I_F(\lambda)$) and the total average lights ($I(\lambda)$). Hence,

$$\alpha_D = ID(\lambda)/I(\lambda) \quad (5)$$

And,

$$\alpha_F = IF(\lambda)/I(\lambda) \quad (6)$$

Rearranging Equation (5) and Equation (6) we get Equation (7) and Equation (8),

$$ID(\lambda) = I\lambda * \alpha_D \quad (7)$$

$$IF(\lambda) = I\lambda * \alpha_F \quad (8)$$

If Equation (7) and Equation (8) were substituted in Equation (4) we get the following identity (Equation (9)):

$$\alpha_D + \alpha_F = 1 \quad (9)$$

Substituting Equation (7) and Equation (8) in Equation (3) we get the following Equation (10).

$$IT\lambda = I\lambda * \alpha_D * \cos\Phi + [I\lambda * \alpha_F] \quad (10)$$

Now rearranging Equation (9) to get expression for α_F and substituting that in Equation (10) we get Equation (11),

$$IT\lambda = I\lambda * [\alpha_D * \cos\Phi + (1 - \alpha_D)] \quad (11)$$

Rearranging Equation (11) to obtain expression for $I(\lambda)$ in terms of $I_T(\lambda)$, α_D and Φ (Equation (12)),

$$I\lambda = IT\lambda / [\alpha_D * \cos\Phi + (1 - \alpha_D)] \quad (12)$$

Substituting Equation (12) in Equation (1) and rearranging we get Equation (13),

$$\rho\lambda IT\lambda = R\lambda [\alpha_D * \cos\Phi + (1 - \alpha_D)] \quad (13)$$

Equation (13) represents the spatially as well as geometrically corrected image. Equation (13) suggests that if the reflectance image of the fruit ($\rho(\lambda)$) is divided by the illumination model which considers the spherical geometry of the fruit ($I_T(\lambda)$), we achieve the spatial and geometrical correction of the image. The expression on the right hand side of Equation (13) proposes that we can achieve the geometric correction of the spatially corrected image ($R(\lambda)$) by dividing it with the factor of $[\alpha_D * \cos\Phi + (1 - \alpha_D)]$. This expression represented the expression for the geometric correction factor (ε_g) (Equation (14)). Hence,

$$\varepsilon_g = [\alpha_D * \cos\Phi + (1 - \alpha_D)] \quad (14)$$

Rewriting the Equation (13) in terms of geometric correction factor (Equation (15)),

$$\rho\lambda = R\lambda \alpha_D * \cos\Phi + 1 - \alpha_D = R\lambda \varepsilon_g \quad (15)$$

where, $\rho(\lambda)$ is the spatially as well as geometrically corrected image.

Gomez et al. (2007) had defined α_F as the ratio between the average amount of light (across all bands) detected by CCD (levels of grey) at the points those coincide with the perimeter of the fruit and the total average amount of light received by the CCD from the whole fruit. At the perimeter, as the angle of incidence (Φ) is 90 degrees, the only component that provides lighting to the fruit is the fuzzy illumination ($I_F(\lambda)$) while for the entire fruit surface the lighting is the combination of direct ($I_D(\lambda)$) and fuzzy illumination ($I_F(\lambda)$) i.e., $I(\lambda)$. Gomez et al. conducted a study and plotted the value of α_F for different points on the perimeter of the clemenules mandarins and then averaged them for each fruit to get value of α_F for every fruit. Finally the mean value of α_F was computed, by taking the mean of values of α_F for all the fruits, to be 0.4896. Also when he plotted the values of α_F for all the points on the perimeter of one single fruit the values were distributed around the mean value very

close to 0.4896. The mean value of parameter α_D was then calculated from Equation (9) as 0.5104. According to the hypothesis of Gomez et al. (2007), the parameters α_D and α_F were related to the illumination system and not to the objects being captured. Hence the values of these parameters were assumed to be constant during their entire study. In the case of our investigation, the value of α_D was not estimated through tests but it was assumed to be a constant and equal to the mean value obtained by Gomez et al. (2007) during their studies of mandarin (i.e., equal to 0.5104).

2.5 Generating the digital elevation model (DEM)

The geometric correction factor (ϵ_g) was a function of two elements; the parameter α_D which was the ratio direct lights (I_D) and the total average lights (I) and the angle of incidence Φ which was the angle between the beam of direct light and the direction normal to the surface. In order to calculate the angle Φ , we needed to know the Cartesian coordinates (i.e., X, Y and heights) of each pixel of the fruit image. However, from the 2-D image of the fruits we obtained only the X and Y coordinates and not the height of any pixel. Consequently Digital Elevation Model (DEM) was used to produce the 3-D model of the fruit from the 2-D image. The basic assumption in the process of developing this 3-D DEM was that the citrus fruits were quasi-spherical. We can compute the geometric correction factor ϵ_g for each pixel as soon as the model has been constructed and elevations (heights) of each of the pixels have been estimated. However, the DEM should be developed separately for each fruit because of the possible difference in the sizes of different fruits. The subsequent steps should be followed to construct this DEM:

Step one – Locating the center of mass (C_g) of the fruit and determining the interpolation network meridians: In order to locate the center of mass (C_g) of the fruit we first needed to determine the pixels that belonged to the fruit and separated them from the background i.e., to obtain the fruit mask. This mask was extracted from the image by using an algorithm previously developed by Qin et al. (2008). This mask created the black and white binary image with white pixels (value = 1) indicating pixels belonging to fruit while black pixels (value = 0)

represented the background. Once the mask was extracted, the X and Y locations of the pixels on the edge of the mask were identified. Now in order to locate the center of mass, few (n_p) equidistant points on the edge of the mask were selected which were called pilot points. The higher the number of pilot points selected, the more accurate the location of center of mass and the more accurate end results can be obtained. In this study 30 ($n_p = 30$) pilot points were selected on the edge. This was done by translating the edge of the mask to the origin (0, 0) and then grabbing the (X, Y) locations of all the pixels on the edge at an angular step of $(2\pi/n_p-1)$. Then the center of mass was (C_g) calculated using the Equation (16).

$$C_g = 1/n_p * I = 1/n_p P_i \quad (16)$$

where, P_i are the (X, Y) locations of the selected n_p pilot points on the edge. Now the lines joining each of those P_i points and the center of mass (C_g) were the meridians of the interpolation network in the DEM. Figure 2 shows the 30 selected pilot points (P_i) on the edge of the mask of the fruit image, which when connected with the center of mass (C_g) forms the meridians of the interpolation network. The pilot points were highlighted as solid circles while the center of mass was shown by a star.

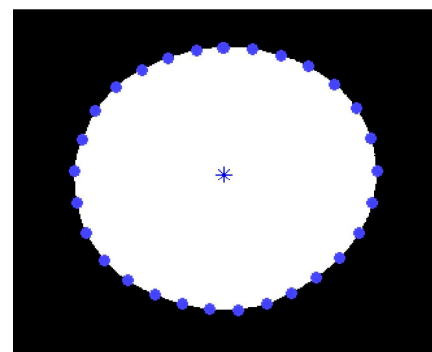


Figure 2 Pilot points and center of mass

Step two – Obtaining the maximum height of the fruit: To facilitate the construction of digital elevation model (DEM) it was mandatory to obtain the height coordinate i.e., elevation of each pixel of the fruit image. To achieve this goal, the maximum height of the fruit was determined and then the elevations of each individual pixel were obtained by interpolation. The maximum height of the fruit was computed from the distance

between the center of mass (C_g) and the pilot points (n_p) using the Equation (17).

$$Hc = 1np * \beta * I = 1np CgPi \quad (17)$$

where, $CgPi$ = Distance between center of mass C_g and pilot point P_i i.e., the radius of the fruit; β = Flattening factor.

As the algorithm may be sensitive to surface irregularities and may result in estimating less spherical shape, the flattening factor was used to take into account such irregularities which were often found in biological products. However in the present study, the flattening factor was assumed to be one for simplicity.

Step three – Determining the elevations of the interpolation network: As mentioned earlier, the elevations of each of the image pixels were calculated using the maximum height of the fruit (h_c). But before that the nodes of interpolation and the interpolation network needed to be obtained. This was done by subdividing each of the radii (C_gP_i) into few numbers of radii segments (r_{ij}) and then locating the interpolation node at the end of each of the segments. The (XY) coordinates of all the nodes were also determined during the process. In the segment r_{ij} , the index ‘i’ varied from 1 to n_p for n_p number of radii ($n_p = 30$ in our case) and the index ‘j’ varied from 1 to the number of segments. In this study, we chose to divide each of the radii into 16 segments. After determining the (XY) coordinates of the nodes, their heights (h_{ij}) were evaluated by modeling the ellipses in the plane formed by each of the radii (C_gP_i) and the maximum height (h_c) of the fruit with (C_gP_i) and h_c to be the semi axes of the ellipse in the respective plane. The following characteristic Equation (18) of ellipse was used to compute the heights of the nodes i.e., h_{ij} .

$$r_{ij}^2 CgPi^2 + h_{ij}^2 h_c^2 = 1 \quad (18)$$

This procedure was repeated for n_p number of times for the n_p number of ellipses formed on the n_p number of planes in order to compute the heights of all the nodes on the n_p number of radii. This resulted in the (X, Y, Z) coordinates for all the interpolation nodes which formed the interpolation network for the DEM.

Step four – Acquiring the elevations of each pixel belonging to fruit by interpolation: After the interpolation

network was formed and the (X, Y, Z) coordinates of all the interpolation nodes were computed, the elevations of all the intermediate pixels of the fruit were obtained by interpolation. The MATLAB commands ‘meshgrid’ and ‘griddata’ were used for the task. The command ‘meshgrid’ was used to duplicate the X and Y coordinates of all the pixels of the fruit image for generating the 3-D model of the fruit. The command ‘griddata’ was used in conjunction with the (X, Y, Z) coordinates of the interpolation nodes in order to obtain the Z or height coordinates i.e., elevations of all the intermediate pixels. After this, the 3-D wireframe parametric surface of the fruit was produced using the MATLAB command ‘mesh’. Then the 3-D digital elevation model (DEM) was generated, the properties of which were then used to estimate geometric correction factor for each fruit pixel.

2.5 Estimation of geometric correction factor

As derived earlier, the geometric correction factor (ϵ_g) is given by the Equation (14). It should be recalled that the geometric correction factor (ϵ_g) was a function of two parameters; the parameter α_D which was the ratio of direct lights (I_D) and the total average lights (I) and the angle of incidence Φ which was the angle between the beam of direct light and the direction normal to the surface. The geometric parameters obtained from the digital elevation model were exploited for estimating the value of angle Φ . The angle Φ was calculated from the spatial coordinates of each pixel (i.e., X, Y, Z Cartesian coordinates) as Equation (19):

$$\tan\Phi = X^2 + Y^2 Z \quad (19)$$

where, Z is the elevation of each pixel (h_{XY}) estimated in the digital elevation model. The geometric correction factor (ϵ_g) was estimated for each pixel using the Equation (14) and Equation (19). The constant α_D was obtained from the work of Gomez et al. (2007) as equal to 0.5104.

After calculating the geometric correction factors (ϵ_g) for all the pixels, each pixel was divided by the corresponding correction factor. One should note that while calculating the center of mass (C_g), the edge of the fruit mask was translated to the origin (0, 0). So while applying the correction factor to each pixel one should take care to divide each pixel by appropriate correction

factor by properly matching the contour of the correction factors with that of the mask.

2.6 Unique contribution: algorithm validation tests

In order to validate the edge effect compensation algorithm tests were conducted using market quality oranges. The novelty of this study lay in the creativity with which the validation tests were designed and the elaborateness of the experiments. Two different experiments were conducted to determine the effectiveness of the algorithm. The first experiment was carried out to prove that the same region of the citrus fruit had similar reflectance in different areas of the image after applying the geometric correction factor. This experiment was conducted by rotating the fruit in steps of approximately 20 degrees and capturing the images at all the locations. The reflectance of the same region of interest in the fruit was measured at different locations and compared. The reflectance measurement was done using ENVI 4.3 software (ITT Visual Information solutions, Boulder, CO USA). The fruits were marked with angular graduations with step size equal to 20 degrees using a black permanent marker. Each fruit was marked with three regions of interest, square in shape and random in size. The images of the fruit at 0, 20 and 40 degrees were captured and the mean reflectance of each of the region was plotted (at 0, 20 and 40 degrees) separately as the reflectance spectra by averaging the reflectance of each pixel included in the region of interest using ENVI 4.3. The pixels in the regions of interest were selected in the zoom window manually, by using various drawing methods (e.g., polygon, rectangle, ellipse, point, grow, and merge etc.). Enough care was taken while selecting the pixels to avoid the edges of the square regions marked with the permanent marker. The reflectance spectra of the region of interest of the fruit, before and after applying the correction factor were compared to identify the effect of applying the correction.

The second experiment included measuring and comparing the reflectance of the market quality orange peel at different locations before and after applying the geometric correction factor. This was done by acquiring the reflectance spectra of the different regions of interest of the fruit over the wavelength range for the study

(450–930 nm) and comparing them. The aim of this trial was to prove that the reflectance of the pixels in different regions of the fruit equalizes or at least the difference between the reflectance of pixels at edge and that of at the center reduces after application of the correction. The technique similar to that of the first test was used for second test also. The three regions of interest were selected in such a way that one was at the center and the other two were closer to the edge. The reflectance of all the three regions of interest at 0, 20 and 40 degrees was plotted in separate plots and compared for evaluating the effect of the correction. The reflectance measurement was done in the same way as that in the first experiment.

3 Results, observations and discussion

3.1 Digital elevation model (DEM) observations

The digital elevation model (DEM) was constructed in order to obtain the geometric parameters needed to compute the geometric correction factor for each pixel. The process was initiated by acquiring the mask of the fruit and choosing 30 pilot points (P_i) on the edge of the mask for computing the center of mass of the fruit. Figure 3 portrays the mask obtained from the fruit image along with the pilot points on the perimeter of the mask. After the pilot points were captured, the meridians of the interpolation network were formed by joining the center of mass (C_g) and all the pilot points (P_i). Once the meridians were in place, the maximum height (h_c) of the elevation model of the fruit was calculated. Each meridian of the interpolation network was then divided into 16 segments (r_{ij}) to obtain the nodes of the interpolation. Figure 3 shows these interpolation nodes (green in color) on one of the meridians of the network along with all the 30 pilot points (red in color) on the perimeter of the fruit.

The elevations of all the nodes were then computed by modeling the ellipses in the plane formed by each of the radii (C_gP_i) and the maximum height (h_c) of the fruit with (C_gP_i) and h_c to be the semi axes of the ellipse in the respective plane. One such transversal plane along with the computed elevations of the respective nodes is demonstrated in Figure 4 below.

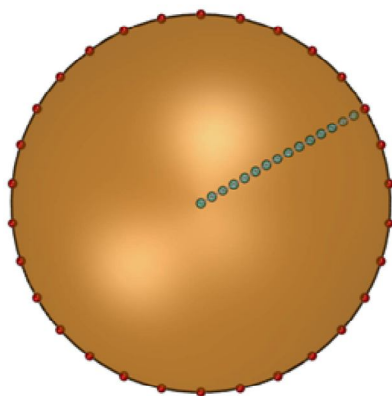


Figure 3 Pilot points (red in color) and nodes of interpolation (green in color) of one of the meridians

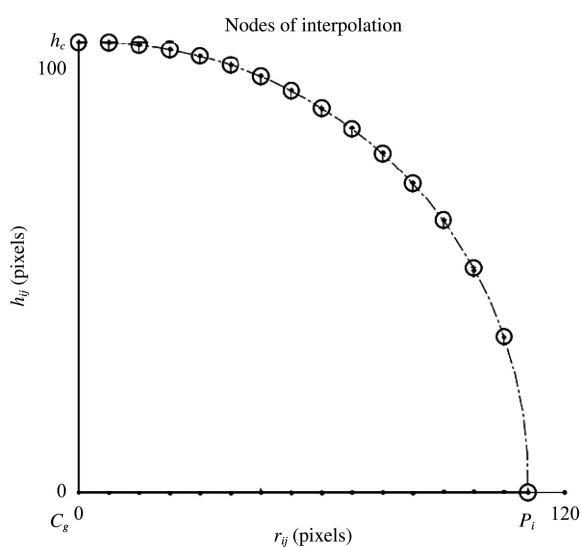


Figure 4 Transversal plane formed by maximum fruit height (h_c) and center of mass of the fruit (C_g). The computed elevation of the interpolation nodes was also shown by ‘center line’

The modeled ellipse with the interpolation nodes on it can be viewed from Figure 5 and Figure 6 which are drawn in Solid Works (2009–2010). Figure 5 is a side view (viewed from direction normal to the transversal plane in which ellipse is modeled) and Figure 6 is the 3-D view of that ellipse. Figure 3 shows the view of Figure 6 taken from top (i.e., top view of Figure 6). The interpolation network was generated as soon as the estimation of elevations of all the nodes on all the meridians were estimated and the (X, Y, Z) coordinates of all the nodes were determined. The construction of interpolation network was followed by the estimation of heights of all the intermediate pixels by interpolation. This concluded the structuring of the digital elevation model.

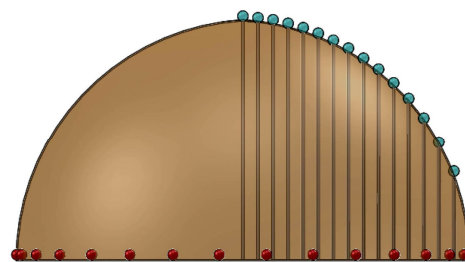


Figure 5 Side view of the modeled ellipse and the elevations of interpolation nodes

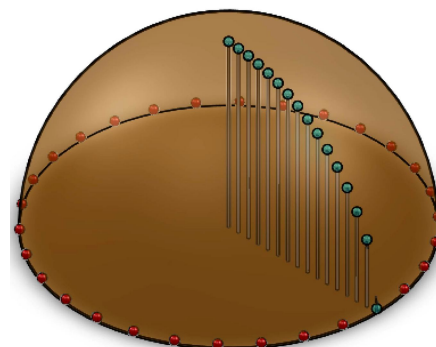


Figure 6 3-D view of the modeled ellipse and the elevations of interpolation nodes

The digital elevation model for one of the fruits is shown in Figure 7.

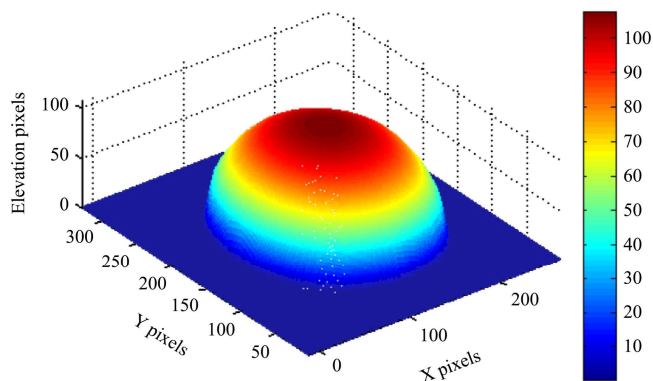


Figure 7 Digital elevation model

3.2 Geometric correction factor observations and results

As noted earlier, the geometric correction factor (ϵ_g) was a function of two elements, the parameter α_D which was the ratio of direct lights (I_D) and the total average lights (I) and the angle of incidence Φ which was the angle between the beam of direct light and the direction normal to the surface. However, as mentioned previously the parameter α_D had been assumed to have a constant value of 0.5104 that was obtained from the work of Gomez et al. (2007) which he computed as the average

value of α_D for different citrus fruit samples. So the geometric correction factor (ϵ_g) only depended on angle of incidence Φ . The angle Φ was calculated for each pixel based on the Cartesian coordinates of that pixel which were obtained from the digital elevation model. The geometric correction factor for each pixel was then plotted in the XY plane to examine its contour. Figure 8 below, shows this contour of the geometric correction factor. When an image of the citrus fruit was captured, the top-center area of the fruit appeared brightest and as one moved towards the fruit edge the image became darker. So when the geometric correction was applied to the image, ideally the pixels at the center of the image should get divided by a factor of 1 as this is the brightest region of the fruit while as one goes away from the center towards edge the geometric correction factor should have lower value. Figure 8 supports the concept mentioned here. The geometric correction factor had the highest value (i.e., 1) in the central region while it was found to be decreasing gradually towards the edge in concentric manner with minimum at edge. Another point to be observed in Figure 8 is that the geometric correction factor of the fruit background (i.e., the pixels in the image that doesn't belong to fruit) is 1 which is logical as these pixels are not required to be corrected.

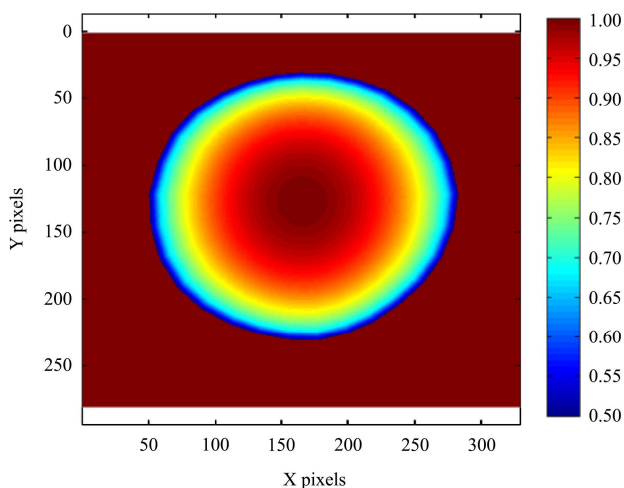


Figure 8 Contour of geometric correction factor (ϵ_g)

The effect of application of the geometric correction to one of the citrus samples (a grape fruit sample from Qin et al. (2008)) is shown in Figure 9. The left image was the citrus fruit before application of the geometric correction while the right one was after application of the

correction. The fruit was affected with canker and the image was captured during prior studies. The image shown was the monochrome image at 724 nm. As can be viewed from the left image, before applying the algorithm the image appeared brighter in the central part while the peripheral area was darker. As discussed earlier, this was because of the spherical geometry of the fruit which resulted in this edge effect. Clearly the image after correction appeared brighter than the one before correction. Also the brightness of the entire image seemed to have more uniformity throughout than the uncorrected image.

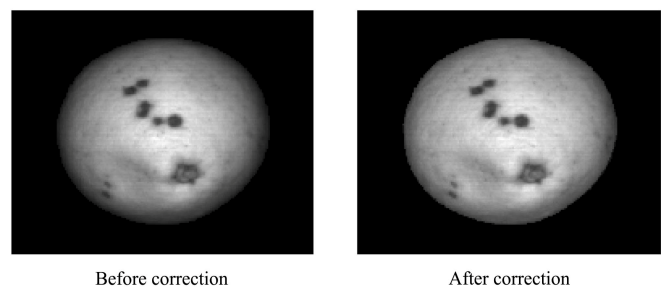


Figure 9 Effect of application of geometric correction-single band image at 724 nm

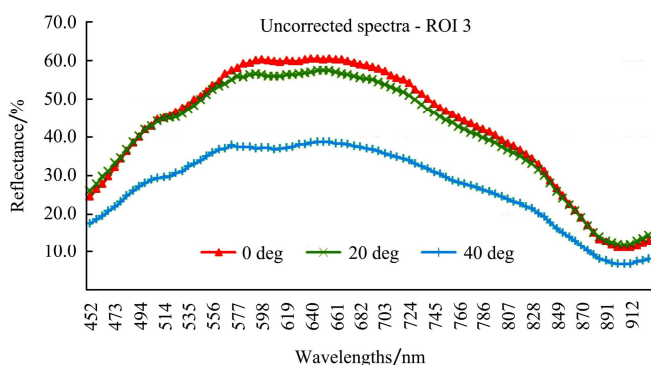
3.3 Validation of test results

The first experiment was to measure and compare the reflectance of the same region of the fruit at different orientations of the fruit, before and after applying the geometric correction. Figure 10 shows one of the fruits (orange) marked with the angular graduations and the regions of interest. The reflectance spectra of all three regions of interest were plotted before and after application of the geometric correction.

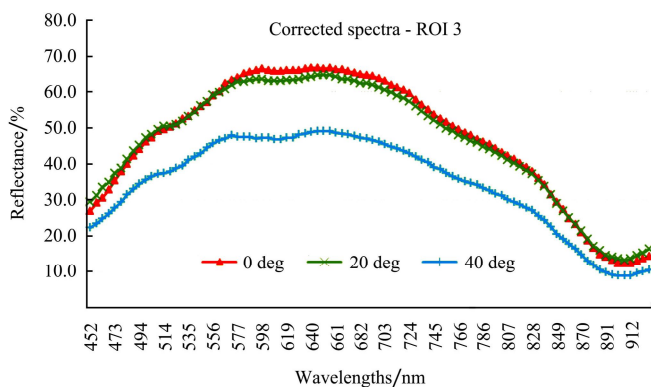
For demonstration purposes the reflectance spectra of region of Interest 3 (ROI 3) are shown in Figures 11a and 11b before and after application of the geometric correction factor respectively. As can be seen from Figure 11a, the reflectance of the ROI 3 at 0 and 20 degrees are pretty close to each other. However the reflectance at 40 degrees was quite lower than the other two. One reason behind this could be the number pixels selected in the region of interest at different angles. At 0 and 20 degrees the pixels selected in the ROI were 385 and 367 respectively; however those selected at 40 degrees were 230.



Figure 10 Citrus sample marked with the angular graduations and the regions of interest



a. Before applying correction



b. After applying correction

Figure 11 Reflectance spectra of ROI 3

A smaller portion of the ROI was visible to the camera as we rotated the fruit by higher angle and hence at 40 degrees a fewer number of pixel were selected. Also it should be noted that the maximum reflectance has occurred at around 660 nm at all three angles. The maximum reflectance at 0 degrees was around 60%, at 20 degrees it was approximately 57% and at 40 degrees it was close to 39%. These observations made sense because as the angle of rotation was increased the portion at top moved closer to the edge in the darkened region (which

was a result of edge effect). Now if one observes the reflectance spectra of ROI 3 after geometric correction in Figure 11b, it can be observed that the maximum reflectance at 0, 20 and 40 degrees is approximately 67%, 65% and 49%, respectively. A significant improvement in the reflectance of the fruit image after the correction was clearly visible from the spectra. Also the difference between reflectance of the region at different orientations can be observed to be reduced after application of the correction. These results demonstrated that the same region of the fruit had similar reflectance in different areas of the image after subjecting it to the geometric correction proposed in the study.

The second experiment consisted of measuring and comparing the reflectance of different regions of the fruit before and after application of the correction. As mentioned earlier three regions were selected on the fruit image, one was at center and two were closer to the edge. The reflectance of all three regions was measured at 0, 20 and 40 degrees. The reflectance spectra of all three regions captured at 40 degrees rotation are shown in Figure 12. Figure 12a shows the spectra before correction and Figure 12b shows after the correction is applied. Obviously the two plots differed from one another. The spectra of the three regions before applying the correction were quite dispersed and they portrayed considerably high degree of variability in spite of being a part of the same homogeneous fruit peel. On the other hand, after correction, the spectra of each region can be seen to be overlapping each other in Figure 12b.

The difference between the reflectance of the three regions has reduced by significant amount. Also if observed carefully the maximum reflectance of ROI 1, 2 and 3 was found to be 45%, 33% and 39% at around 660 nm before correction. After the correction was applied, these numbers increased to 51%, 45% and 49%. These numbers highlighted the consequences of application of geometric correction. At the rotation of 40 degrees, the ROI 1 had curvature only in one direction while ROI 2 and 3 had curvature in two directions, which was the reason behind ROI 1 having highest reflectance out of the three regions. Also after closer examination it was observed that ROI 2 had a little mark of a blue pen

inside it. This might have caused ROI 2 to have the minimum reflectance of all. The fruit being observed had uneven curvature in the regions 2 and 3 which also could have contributed to the different reflectance of the regions. It was concluded after the test, that application of the geometric correction on different regions on the fruit resulted in similar reflectance.

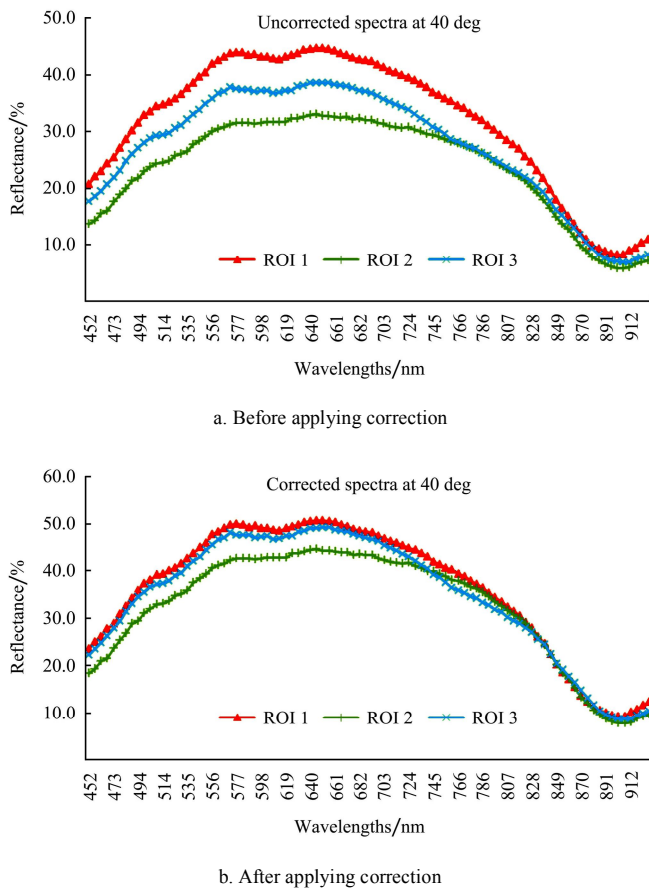


Figure 12 Reflectance spectra of all three ROIs at the rotation of 40 degrees

In the above experiments all three regions represented normal peel conditions on the same fruit belonging to the marketable class. However, the darkening edge effect contrasted the brighter central area, creating confusion in the classification algorithm (which can be seen from the spectra in Figure 12a). The point to be noted here was that, when applying the correction, edge effect variability within the same class reduced significantly (referring to the spectra in Figure 12b). This fact was very important from the point of view of an automatic grading system as it reduced the misclassification rate, regardless of the class of peel conditions being considered. In the later part of the study, five market quality and five cankerous

citrus fruits were used and the first experiment was repeated on them, which consisted of measuring the reflectance of the same region at different orientations (at 0, 20 and 40 degrees) of the fruit. Each marketable fruit was marked with a rectangular region of interest of random size with a black permanent marker; while in case of cankerous fruits, the canker lesions were the regions of interest. The reflectance spectra of the region of interest (ROI) of one of the cankerous orange at different orientations, is shown in Figure 13. In this case the canker lesion was approximately 13-15 mm in diameter. While measuring the reflectance of this ROI care was taken to maintain its purity (no edges or normal peel were included). Figure 13a shows the reflectance spectra of the cankerous orange before applying the correction while Figure 1b shows that after correction. The results observed were similar to those observed in Figure 11. As can be seen in Figure 13a the reflectance of the ROI at 0 degrees is higher than that at 20 and 40 degrees. The maximum reflectance at all the orientations has appeared at 813 nm. At 0 degrees the maximum reflectance of the canker ROI was

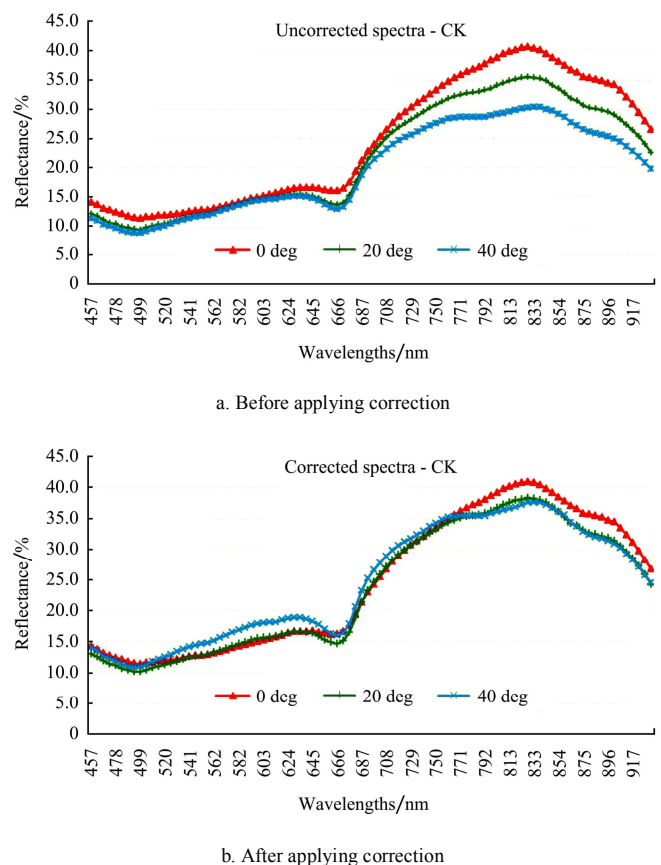


Figure 13 Reflectance spectra of Canker ROI

approximately 40% and that at 20 and 40 degrees was approximately 35% and 30% respectively. After geometric correction the reflectance at 20 and 40 degrees was improved and was found to be very close to that at 0 degrees (approximately 40%). This can be seen in Figure 13b, where reflectance spectra at different orientations almost overlap each other.

4 Conclusion

Florida citrus industry is a major contributor to the economy of the State of Florida. Meanwhile, the Florida citrus industry has been facing the consequences of canker for nearly a decade. Attempts to identify diseased citrus fruits and prevent them from entering canker-free areas inside and outside United States have primarily been done by human inspectors. Automatic disease detection systems using computer vision, image processing and pattern recognition techniques have proven themselves to be very effective in identifying and separating cankerous citrus fruits from other peel conditions. However, one of the major concerns when every computer vision system capturing and processing images of a spherical object was the edge effect. This edge effect may cause the segregation algorithm to misclassify normal healthy fruit peel as disease due to darkening of the edges.

A model to compensate for this edge effect was implemented following the study of Gomez et al. (2007) during this exploration. The algorithm assumed the fruit to be a Lambertian ellipsoidal surface. With this assumption, a 3-D digital elevation model of the fruit was developed from its 2-D image. The Cartesian coordinates (X, Y and Z) of each pixel on the fruit surface were determined from the digital elevation model. These coordinates were used to estimate the geometric correction factor (ε_g) for each pixel. When the reflectance of each pixel was divided by the corresponding correction

factor (ε_g), the image corrected for the curvature effect of the spherical object was obtained. During the process of correction, the value of α_D from Gomez et al. (2007) was assumed, yielding excellent image enhancement. As a consequence of this geometric correction it became feasible to retrieve the portion of the reflected signal that was lost while capturing an image of a spherical object due to its curvature. The true reflectance can then be estimated by equalizing the intensity of radiation over the whole surface of the fruit, which tended to minimize edge effects. Additional experiments were conducted to show that the reflectance became more uniform over the fruit surface thus correcting the image for geometric variation. Fruit peel segments from healthy and diseased fruit demonstrated a significant improvement in reflectance spectra after compensation at three different orientations around the fruit.

One disadvantage of this method is that each fruit has to be treated separately in order to create the digital elevation model. Since only one fruit can be processed at a time with this methodology, it is time consuming and thus computationally expensive. If the algorithm is implemented in a real time online application it may demand a considerably faster processor. Future work should seek to develop an optimized compensation approach suitable for real-time applications.

Acknowledgement

The authors gratefully acknowledge the financial support of Florida Fresh Packer Association and USDA Technical Assistance for Specialty Crops. The authors would also like to thank Dr. Duke Bulanon of University of Florida for his assistance while conducting the experiments. Finally the authors would like to extend their gratitude to Mr. Mike Zingaro and Mr. Greg Pugh of University of Florida for building the hyperspectral imaging system.

References

- Aleixos, N., J. Blasco, F. Navarrón, and E.Moltó. 2002. Multispectral inspection of citrus in real-time using machine vision and digital signal processors. *Computers and Electronics in Agriculture*, 33 (2002): 121–137.
- Cheng, X., Y. R. Chen, Y. Tao, C. Y. Wang, M. S. Kim, and A. M. Lefcourt. 2004. A novel integrated PCA and FLD method on hyperspectral image feature extraction for cucumber chilling

- damage inspection. Information and Electrical Technologies Division of ASAE. ISSN 0001-2351. 47(4): 1313-1320.
- Chen, Y. R., K. Chao, and M. S. Kim. 2002. Machine vision technology for agricultural applications. *Computers and Electronics in Agriculture*, 36(2002): 173-191.
- Das, A. K. 2003. Citrus canker – A review. *Journal of Applied Hort*, 5(1): 52-60.
- Foley, J., A. Feiner, S. Van Dam, and J. Hughes. 1996. *Computer Graphics: Principles and Practice*. Second Edition.
- Gómez-Sanchis, J., E. Molto, G. Camps-Valls, L. Gómez-Chova, N. Aleixos, and J. Blasco. 2008. Automatic correction of the effects of the light source on spherical objects. An application to the analysis of hyperspectral images of citrus fruits. *Journal of Food Engineering*, 8 (2008): 191-200.
- Gonzalez, R., R. Woods, and S. Editions. 2004. *Digital image processing using MATLAB*.
- Hodge, A., E. Philippakos, D. Mulkey, T. Spreen, and R. Muraro. 2001. Economic impact of Florida's citrus industry, Extension Digital Information Source (EDIS) FE307. Gainesville, Florida: University of Florida, Department of Food and Resource Economics, 1999-2000.
- Kim, M. S., A. M. Lefcourt, K. Chao, Y. R. Chen, I. Kim, and D. E. Chan. 2002. Multispectral detection of fecal contamination on apples based on hyperspectral imagery: Part I. Application of visible and near-infrared reflectance imaging. *Transactions of ASAE*, 45(6): 2027-2037.
- Kim, M. S., Y. R. Chen, P. M. Mehl. 2001. Hyperspectral reflectance and fluorescence imaging system for food quality and safety. ASAE ISSN 0001-2351.
- Kim, M. S., A. M. Lefcourt, Y. R. Chen, I. Kim, D. E. Chan, and K. Chao. 2002. Multispectral detection of fecal contamination on apples based on hyperspectral imagery: Part II. Application of hyperspectral fluorescence imaging. Information and Electrical Technologies Division of ASAE. ISSN 0001-2351. 45(6): 2039-2047.
- Kim, D. G., T. F. Burks, J. Qin, and D. M. Bulanon. 2009. Classification of grapefruit peel diseases using color texture feature analysis. *International Journal of Agricultural & Biological Engineering*, 2(3): 41-50.
- Koschan, A. and M. Abidi. 2008. *Digital Color Image Processing*, First Edition.
- Lee, K., S. Kang, S. R. Delwiche, M. S. Kim, and S. Noh. 2008. Correlation analysis of hyperspectral imagery for multispectral wavelength selection for detection of defects on apples. *Sensing and Instrumentation for Food Quality and Safety*, 2(2): 90-96.
- Lu, R. 2008. Quality evaluation of fruit by hyperspectral imaging. Chapter in *Computer vision technology in food quality evaluation*.
- Lu, R. 2002. Detection of bruises on apples using Near-Infrared hyperspectral imaging. Information and Electrical technologies Division of ASAE ISSN 0001-2351. 46(2): 523-530.
- Noordam, J. C., W. HAM van den Broek, and L. M. C. Buydens. 2005. Detection and classification of latent defects and diseases on raw French fries with multispectral imaging. *Journal of the Science of Food and Agriculture*, 85(2005): 2249-2259.
- Park, B., K. C. Lawrence, W. R. Windham, and R. J. Buhr. 2002. Hyperspectral imaging for detecting fecal and ingesta contaminants on poultry carcasses. ASAE ISSN 0001-2351.
- Park, B., Y. R. Chen, and M. Nguyen. 1997. Multispectral image analysis using neural network algorithm for inspection of poultry carcasses. *Journal of Agricultural Engineering Research*, 69(1998): 351-363.
- Park, B., and Y. R. Chen. 2000. Co-occurrence matrix texture features of multispectral images on poultry carcasses. *Journal of Agricultural Engineering Research*, 78(2): 127-139.
- Pydipati, R., T. F. Burks, and W. S. Lee. 2005. Statistical and neural network classifiers for citrus disease detection using machine vision. Information and Electronics Technologies Division of ASAE. ISSN 0001-2351. 48(5): 2007-2014.
- Pydipati, R., T. F. Burks, and W. S. Lee. 2006. Identification of citrus disease using color texture features and discriminant analysis. *Computers and Electronics in Agriculture*, 52(1-2): 49-59.
- Piron, A., V. Leemans, O. Kleynen, F. Lebeau, and M. F. Destain. 2007. Selection of the most efficient wavelength bands for discriminating weeds from crop. *Computers and Electronics in Agriculture*, 62 (2008): 141-148.
- Qin, J., T. F. Burks, M. S. Kim, K. Chao, and M. A. Ritenour. 2008. Citrus canker detection using hyperspectral reflectance imaging and PCA-based image classification method. *Sensing and Instrumentation for Food Quality and Safety*, 2(3): 168-177.
- Qin, J., T. F. Burks, M. A. Ritenour, and W. G. Bonn. 2009. Detection of citrus canker using hyperspectral reflectance imaging with spectral information divergence. *Journal of Food Engineering*, 93(2): 183-191.
- Qin, J., T. F. Burks, X. Zhao, N. Niphadkar, and M. A. Ritenour. 2011a. Hyperspectral band selection for multispectral detection of citrus canker. *Transactions of ASABE*, 54(6)1-11.
- Qin, J., T. F. Burks, X. Zhao, N. Niphadkar, and M. A. Ritenour. 2011b. Development of a two-band spectral imaging system for real-time citrus canker detection. *Journal of Food Engineering*, 108(2012): 87-93.
- Schubert, T. S. and J. W. Miller. 2000. Bacterial citrus canker. FDACS, Division of plant industry, Gainesville, Florida. 6 fold.
- Shirai, Y., N. Kondo, and T. Fujiura. 1998. Machine vision. Chapter in *Robotics for bioproduction systems*.
- The Imaging Source: Manufacturer of industrial machine vision cameras. How color cameras work? Available at: http://www.theimagingsource.com/downloads/howcolcamswp_en_US.pdf. Accessed 19 January 2010.
- Unay, D. and B. Gosselin. 2006. Stem and calyx recognition on 'Jonagold' apples by pattern recognition. *Journal of Food Engineering*, 78 (2007): 597-605.